DE-AC02-76SF00515 DE-FG02-91ER-40622 SLAC-PUB-10756

DPF 2003: Annual Meeting of the Division of Particles and Fields of the American Physical Society
5-8 April 2003, Philadelphia, Pennsylvania

Study of B Decays into the Final State $D^{(*)}\pi\pi\pi$ at $BABAR$

H. W. Zhao
University of Mississippi–Oxford

Based on a data sample of an integrated luminosity of 57.4 fb^{-1} at the $\Upsilon(4S)$ resonance taken with the *BABAR* detector using the SLAC PEP-II asymmetric-energy B-Factory, hadronic decays of B meson with the final states $D^{(*)}$ and three pions are studied. The study is performed by fully reconstructing the exclusive decays of $B \to D^{(*)}a_1(1260)$ and the non-resonant modes $B \to D^{(*)}\rho^0\pi$ and $B \to D^{(*)}\pi\pi\pi$. The current status of the study is presented and a dominant $B \to D^{(*)}a_1(1260)$ decay is shown.

I. INTRODUCTION

Hadronic B decays provide important information on both the weak and hadronic interactions of heavy flavored mesons. The quarks produced in such nonleptonic weak decays can arrange themselves into hadrons in many ways. The final state is linked to the initial state by QCD processes. The theoretical description of hadronic decays of heavy mesons invoke the factorization approximation and heavy quark effective theory (HQET) [1].

The dominant hadronic decay modes of the B meson involve tree-level diagrams where the $b \to c$ transition leads to a charmed meson and an external W boson, which often emerges as a charged meson π, ρ or $a_1(1260)$. In the models based on the Bauer-Stech-Wirbel approach [1,2], two parameters a_1 and a_2, which describe the QCD hard-gluon corrections for external and internal spectator processes respectively, provide important clues into the role played by the strong interaction in these two-body tree-level decays. Parameters a_1 and a_2 are expected to be process dependent, but previous experimental data can be described with universal values ($a_1 \approx 1$ and $a_2 \approx 0.2$). Recent results of $B^0 \to \bar{D}^{(*)0}\pi^0$ from CLEO and Belle (both indicate a_2 to be ≈ 0.4) begin to show the expected process dependence of a_2 [3,4]. A precise measurement of B decaying to $D^{(*)}a_1(1260)$ provides an interesting approach to estimate the constants a_1 and a_2 and to test the factorization hypothesis. Since the QCD interaction between the product quarks continues after the weak transition takes place and after hadron formation, an understanding of final state interactions (FSI) is very important. The study of the non-resonant modes $B \to D^{(*)}\rho^0\pi$ and $B \to D^{(*)}\pi\pi\pi$ may provide important information on this mechanism.

Hadronic B decays also play a significant role in CP violation study. A precise measurement of $B^0 \to D^{(*)-}a_1^+$ is important in measuring $\sin(2\beta+\gamma)$, where β and γ are the angles of the Unitary Triangle related to the CP asymmetries in B decay [5]. Presently $B^0 \to D^{*-}a_1^+$ is also suggested as a test of chirality [6].

Studies of $B \to D^{(*)}a_1$ and of their non-resonant decays were previously performed by CLEO and ARGUS [7,8,9,10]. Because of limited statistics, the uncertainties of the branching fraction measurements are relatively large [11], and some of the detailed substructure of the resonance is not available. *BABAR* has collected a large data sample of $B\bar{B}$ pairs at the PEP-II B-Factory [12], making possible an improved study of these modes.

In this paper we present the status of our study. The *BABAR* detector and data are described in Section II, and the event selection with data analysis is presented in Section III. A summary is given in Section IV. Charge conjugation is always implied in this report.

II. THE *BABAR* DETECTOR AND DATA SET

The data used in this analysis consists of 62.2 million $B\bar{B}$ pairs, corresponding to an integrated luminosity of 57.4 fb^{-1}, collected with the *BABAR* detector at the $\Upsilon(4S)$ resonance. The *BABAR* detector [13] was constructed

to observe CP violation and was motivated by the measurements of B^0 mixing made almost two decades ago [14]. Charged particles are reconstructed with a five layer, double-sided silicon vertex tracker (SVT) [15] and a 40 layer drift chamber (DCH) with a helium-based gas mixture [16], placed in a 1.5 T solenoidal field produced by a superconducting magnet. The charged particle momentum resolution is approximately $(\delta p_T)^2 = (0.0013 p_T)^2 + (0.0045)^2$, where p_T is given in GeV/c. The SVT, with a typical single-hit resolution of 10 μm, provides measurement of impact parameters of charged particle tracks in both the plane transverse to the beam direction and along the beam. Charged particle types are identified from the ionization energy loss (dE/dx) measured in the DCH and SVT, and the Cherenkov device (DIRC) [17]. Photons are identified by a CsI(Tl) electromagnetic calorimeter (EMC) with an energy resolution $\sigma(E)/E = 0.023 \cdot (E/\mathrm{GeV})^{-1/4} \oplus 0.019$ [18].

III. EVENT SELECTION AND DATA ANALYSIS

B mesons are reconstructed in modes of B decaying to $D^{(*)}$ and three pions, which may form the resonance $a_1(1260)$ and non-resonant $\rho^0\pi$ and $\pi\pi\pi$. They contain $B^0 \to D^{*-}a_1^+$, $B^+ \to \bar{D}^{*0}a_1^+$, $B^0 \to D^-a_1^+$, $B^+ \to \bar{D}^0 a_1^+$, and their corresponding non-resonant modes $D^{(*)}\rho^0\pi$ and $D^{(*)}\pi\pi\pi$.

To reconstruct the charmed mesons D and D^* and the light mesons in the final states, the charged tracks are required to have a distance of closest approach within $\pm$10 cm in z and 1.5 cm in radius of the average beam spot position, and at least 12 hits recorded in the DCH. Kaons and pions are selected, depending on their track's momentum, based on the dE/dx information from the SVT and DCH, as well as the Cherenkov angle and the number of photons measured with the DIRC. For each detector component d = (SVT, DCH, DIRC), a likelihood L_d^K (L_d^π) is calculated given the kaon (pion) mass hypothesis. Photons are selected as showers in the calorimeter that have a lateral shower shape consistent with the expected pattern of energy deposits for an electromagnetic shower and with an energy $E_\gamma > 30$ MeV.

The D^0 meson is selected from the decays $K^-\pi^+$, $K^-\pi^+\pi^0$ and $K^-\pi^+\pi^-\pi^+$, while the D^+ meson is selected from $K^-\pi^+\pi^+$ and $K^0_S\pi^+$ modes. The track momentum is required to be greater than 200 MeV/c. π^0s are reconstructed from two photons with the sum of their energies $E_{\gamma\gamma}$ greater than 200 MeV/c and an invariant mass 0.120 GeV/c^2 $< m_{\gamma\gamma} <$ 0.150 GeV/c^2 (about $\pm$2.5 times the resolution of the π^0 invariant mass). A mass constraint fit is applied to π^0 candidates, which improves the energy resolution from 2.4% to 1.8%. K^0_S mesons are reconstructed from two pion tracks with opposite charge. The invariant mass of the candidate $\pi^+\pi^-$ is required to be $|m_{\pi\pi} - 497.7$ MeV/c^2 $| < 15.0$ MeV/c^2 and the momentum of the K^0_S greater than 200 MeV. In K^0_S selection the angle between the flight direction, which is the vector which points from the primary vertex to the $\pi^+\pi^-$ candidate's vertex, and the direction of the $\pi^+\pi^-$ candidate's three momentum is used as a cut. A vertex fit is applied, and a probability of χ^2 greater than 0.1% is required. The invariant mass of the candidate of $D^0 \to K^-\pi^+$, $K^-\pi^+\pi^-\pi^+$, and $D^+ \to K^-\pi^+\pi^+$, $K^0_S\pi^+$ is required to be within 3σ from the true value of the mass. As the combinatorial background of the $D^0 \to K^-\pi^+\pi^0$ is larger due to the presence of the π^0, a 2σ mass cut is applied on this mode. The tracks of the D meson are required to originate from the same point; therefore a vertex fit is applied with the requirement of a probability of χ^2 greater than 0.1%. Then a combined vertex and mass constraint fit is applied and a convergent fit is required. The mass-constraint fit changes the momenta of the D meson daughters forcing the invariant mass to be the nominal one, thus improving the D energy and momentum resolutions.

Reconstructed D^0s are combined with soft pions π^- (π^0) to form D^{*-} (D^{*0}) candidates. The soft pion momentum is required to be less than 450 MeV/c. The requirements of $E_{\gamma\gamma} > 200$ MeV for π^0 and the minimum momentum requirement of 200 MeV/c for the pion are removed for soft pions. D^* candidates are selected by the requirement that the mass difference between D^* and D^0, $\Delta m = m_{D^*} - m_{D^0}$, lies within $\pm 3\sigma$ (σ is the resolution of Δm) of the nominal mass difference. Then $D^{*+} \to D^0\pi^+$ candidates are refitted with the beam-spot constraint to improve the angular resolution for the soft pion, and a convergent combined vertex and mass constraint fit is also applied. For $D^{*0} \to D^0\pi^0$, no vertex fit is applied, but a kinematic and mass constraint fit are applied and required to be convergent.

ρ^0 mesons are reconstructed from $\pi^+\pi^-$ pairs with the requirement of pion momenta greater than 200 MeV/c and the invariant mass satisfying $|M_{\pi^+\pi^-} - 0.770$ GeV/c^2 $| < 0.15$ GeV/c^2. $a_1^\pm$ mesons are reconstructed by combining the selected ρ^0 and a pion with the pion momentum greater than 200 MeV/c and the invariant mass $m_{\rho^0\pi^\pm}$ to be between 1.0 GeV/c^2 and 1.6 GeV/c^2. A vertex fit is applied to the candidates of ρ^0 and $a_1^\pm$, and a χ^2 probability greater than 0.1% is required.

The B^0 and B^+ mesons are reconstructed by combining selected D or D^* with a_1 candidates, $\rho^0\pi$ or $\pi\pi\pi$. The variables ΔE and m_{ES} are used to define the B signal. $\Delta E = E_B^* - E_{beam}^*$ is the energy difference between the energy of the B candidate and the beam energy in the $\Upsilon(4S)$ system, i.e., E_B^* is the center of mass energy of the B candidate and E_{beam}^* is the center of mass beam energy. The B signal is expected to peak at $|\Delta E| = 0$. The beam energy substituted mass of B candidate, m_{ES}, is defined as $m_{ES} = \sqrt{E_{beam}^2 - (\sum_i \vec{p}_i^*)^2}$ where $\vec{p}_i^*$ is the center of mass momentum of the i-th daughter of the B candidate. The resolution in this variable is limited by the beam energy spread, which is about 2.7 MeV for *BABAR*. Since the final states involve many tracks and more than one candidate can be found in the event, the combinatorial background is high. To suppress such background, we chose for each mode the B candidates whose daughter D or D^* masses are most consistent with their nominal given masses. Then among them the candidate with smallest $|\Delta E|$ is selected. This selection will remove most of the combinatorial background and keep the best candidates.

One major source of background comes from the $q\bar{q}$ continuum background. The continuum background is due to the large non-resonant fraction of the hadronic cross-section, approximately 75% at the $\Upsilon(4S)$, from direct $e^+e^- \to q\bar{q}$ $(q = c, s, u, d)$. To select $B\bar{B}$ events from $\Upsilon(4S)$ data and reduce the continuum background, the ratio of second to zeroth Fox-Wolfram moment, R_2, is used [19]. In the rest frame of $\Upsilon(4S)$, R_2 approaches zero for spherical events and one for jet-like events (Fig. 1). $R_2 < 0.4$ is required in event selection since the momenta of B's are very small and $B\bar{B}$ events are spherical, whereas $q\bar{q}$ continuum events are jet-like in the frame of $\Upsilon(4S)$.

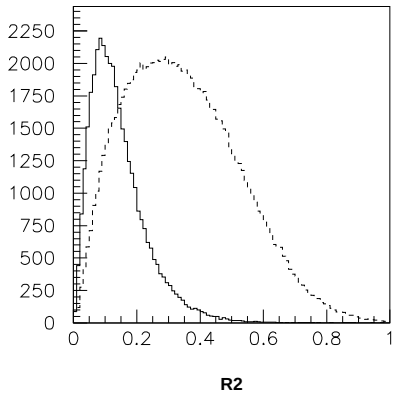

FIG. 1. Distribution of R_2. The solid-line distribution is for $B\bar{B}$ Monte Carlo events and the dashed-line distribution is for continuum $q\bar{q}$ Monte Carlo events.

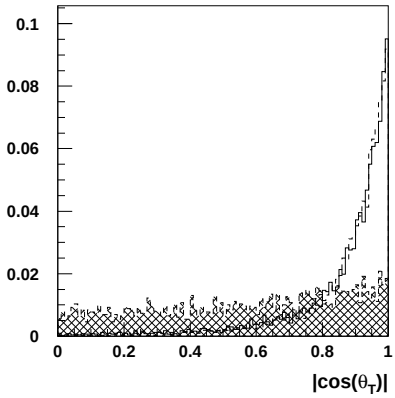

FIG. 2. Normalized distribution of $|\cos(\theta_T)|$. The hatched area is the distribution for $B\bar{B}$ Monte Carlo events. The solid-line and dashed-line histograms are for continuum $c\bar{c}$ and $q\bar{q}$ $(q = u, d, s)$ Monte Carlo events respectively. (The vertical axis has arbitrary units).

The thrust angle θ_T, which is the angle between the thrust axis of the B candidate and the thrust axis of the remaining tracks in the event, is also used to suppress the continuum background. Monte Carlo simulation shows that the distribution of the thrust angle for continuum background events and of $B\bar{B}$ events are quite different (Fig. 2). The distribution of $|\cos(\theta_T)|$ is flat for $B\bar{B}$ events and peaks at 1.0 for continuum $q\bar{q}$ events. We require $|\cos(\theta_T)| < 0.70$ for the $B^- \to D^0 a_1^-$, $D^0\rho^0\pi^-$ and $D^0\pi^+\pi^-\pi^-$ modes with $|cos(\theta_T)| < 0.85$ for all other modes.

A. Resonant mode $B^{(*)} \to D^{(*)}a_1(1260)$

In this decay B mesons are selected in the modes $B^0 \to D^{*-}a_1^+$, $B^+ \to \bar{D}^{*0}a_1^+$, $B^0 \to D^-a_1^+$ and $B^+ \to \bar{D}^0 a_1^+$. The a_1^+ meson is a very broad ($\Gamma \approx 400$ MeV) isovector ($I = 1$) state with $l = 1$ orbital excitation and $J^P = 1^+$. Fig. 3 shows the Monte Carlo simulated spectra of a_1^+ mass and momenta in the decay of $B \to D^{(*)}a_1(1260)$. a_1^+ are reconstructed from a combination of selected ρ^0 and a charged pion, with the pion momentum greater than 200 MeV/c and the invariant mass $m_{\rho^0\pi^\pm}$ between 1.0 GeV/c^2 and 1.6 GeV/c^2 consistent with the a_1^+ mass. An additional cut on the center of mass momentum of the a_1 candidate is applied with $p_{a_1}^* > 0.5$ GeV/c. A vertex fit is performed and a χ^2 probability greater than 0.1% is required. All selected D^0 and D^+ candidates from B decays or D^* decays are required

to have a momentum p^*_D in the $\Upsilon(4S)$ frame greater than 1.3 GeV/c. The ΔE distributions for $B \to D^{(*)}a_1(1260)$ with $m_{ES} > 5.27$ GeV/c^2 are shown in Fig. 4, while the m_{ES} distributions with $|\Delta E| < 2.5\sigma_{\Delta E}$ are shown in Fig. 5 and Fig. 6.

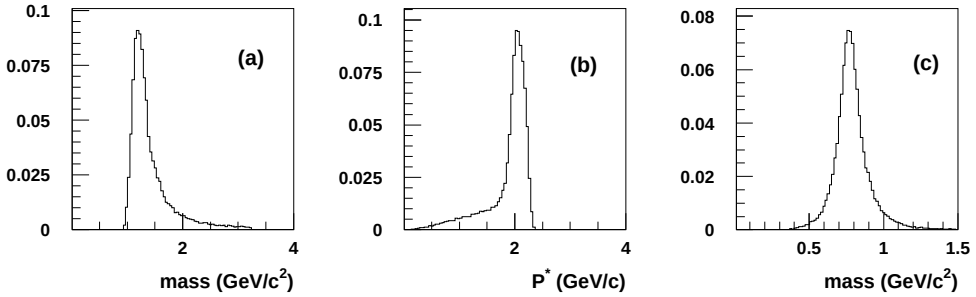

FIG. 3. Monte Carlo simulated spectra (normalized distribution with arbitrary unit invertical axis) for (a) a_1^+ mass and (b) momenta in the decay of $B \to D^{(*)}a_1(1260)$, and (c) the mass of ρ^0 from a_1.

The m_{ES} background can be separated into continuum and $B\bar{B}$ components. The $B\bar{B}$ background component is the result of mis-reconstructing other $B\bar{B}$ decays. The relative contributions and the overall amount of background varies decay-mode by decay-mode depending primarily on the multiplicity of the B decay. We use generic Monte Carlo $B\bar{B}$ data with the signal modes $B \to D^{(*)}a_1$ and non-resonant modes $B \to D^{(*)}\rho^0\pi$ and $B \to D^{(*)}\pi\pi\pi$ removed, and continuum Monte Carlo $q\bar{q}$ data to model the background and find that the background shape of data can be well characterized by Monte Carlo (Fig. 7). The Monte Carlo backgrounds are fitted to an Argus function [20] and the obtained shape parameters of such functions are used in the fitting of m_{ES} of data as shown in Fig. 5 and Fig. 6.

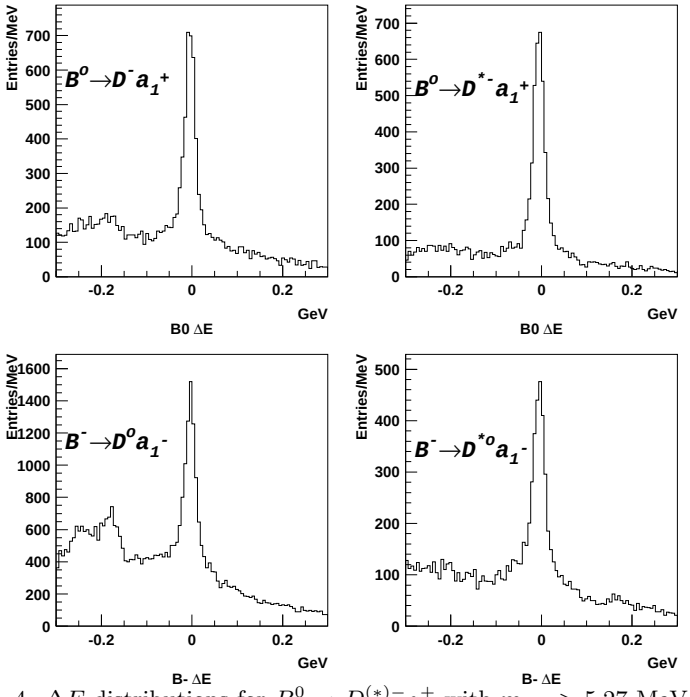

FIG. 4. ΔE distributions for $B^0 \to D^{(*)-}a_1^+$ with $m_{ES} > 5.27$ MeV/c^2.

In the signal region of $B \to D^{(*)}a_1$, some events of the non-resonant decays of $B \to D^{(*)}\rho^0\pi$ and $B \to D^{(*)}\pi\pi\pi$ can pass the event selection criteria of $B \to D^{(*)}a_1$ and form a peaking background. This is confirmed by $B\bar{B}$ Monte Carlo data. Fig. 8 shows that peaking background of all the non-resonant modes underlays the Monte Carlo signal of $B \to D^{(*)}a_1$. The estimation of contributions from non-resonant modes to $B \to D^{(*)}a_1$ modes will be given in the next subsection. It is also possible that the decay of $B^0 \to D^{*-}\pi^+\pi^+$ may pollute the signal of $B^- \to D^0a_1^-$ by misreconstructing ρ^0 from one direct π^+ and the slow π^- from D^{*-}, where the mass of $\rho^0\pi^+$ lies in the a_1 region. Monte Carlo study shows that compared with the decays $B \to D^*\rho^0\pi^-$ and $B \to D^*\pi^-\pi^+\pi^-$, its contribution is quite small and can be neglected. Another possible source of background is from the decay $B^- \to D_1^0(2420)\pi^-$ (ρ^-) and $B^- \to D_2^0(2460)\pi^-$ (ρ^-), where D_1^0 or D_2^0 decays to $D^{*+}\pi^-$ [21]. Monte Carlo study also shows that their

contributions are quite small and can be neglected.

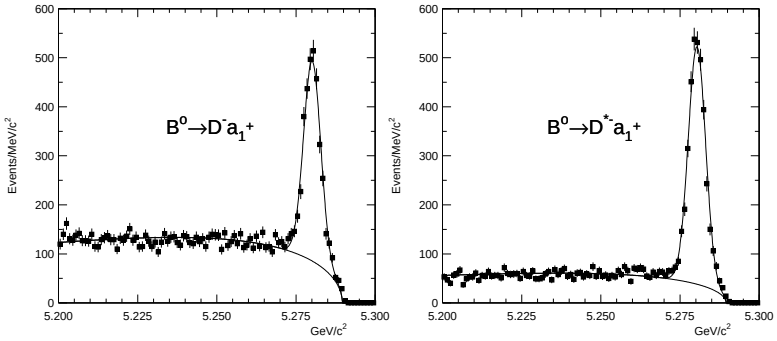

FIG. 5. m_{ES} distributions for $B^0 \to D^{(*)-} a_1^+$ with $|\Delta E| < 2.5\sigma_{\Delta E}$.

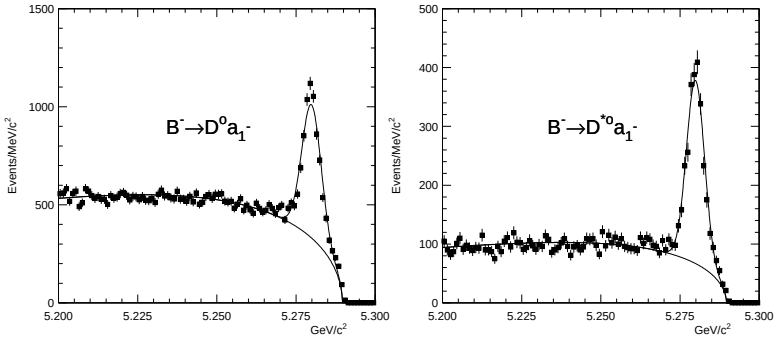

FIG. 6. m_{ES} distributions for $B^- \to D^{(*)0} a_1^-$ with $|\Delta E| < 2.5\sigma_{\Delta E}$.

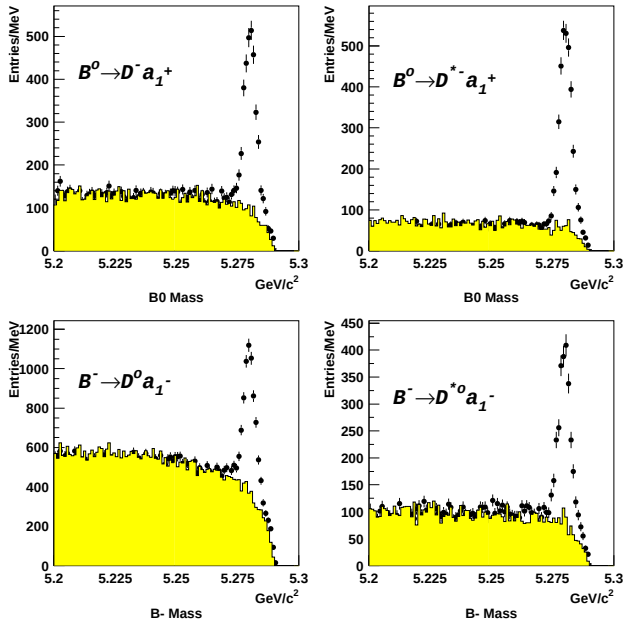

FIG. 7. m_{ES} distributions of $B \to D^{(*)} a_1$ from data (dots) and background modeled by Monte Carlo (shaded area).

The event selection efficiencies for each submode have been studied using signal Monte Carlo data and are reported in Table 1. Estimates of the statistical and systematic error of branching fraction measurements are also listed in the table. The systematic error is mainly considered from the following sources (1) the branching fraction errors of intermediate decays, (2) the error of the integrated luminosity (about 1.1%), (3) the error on the acceptance efficiency due to Monte Carlo statistics, and (4) the error on the charged track reconstruction efficiency, which is 1.2% per

charged track. An additional error of 1.6% is added in quadrature to account for the uncertainty in the soft pion reconstruction efficiency.

TABLE I. Event selection efficiencies and branching fraction error estimation.

B mode	D mode	ε_{MC}	$\Delta BF/BF$ (stat.)	$\Delta BF/BF$ (syst.)
$D^{*+}a_1^-$	$K^-\pi^+$	9.9%		
	$K^-\pi^+\pi^0$	3.4%	3.4%	8.6%
	$K^-\pi^+\pi^+\pi^-$	4.9%		
$D^+a_1^-$	$K^-\pi^+\pi^+$	8.3%	3.0%	9.5%
	$K^0_S\pi^+$	8.0%		
$D^{*0}a_1^-$	$K^-\pi^+$	5.9%		
	$K^-\pi^+\pi^0$	2.0%	4.5%	11.5%
	$K^-\pi^+\pi^+\pi^-$	2.7%		
$D^0a_1^-$	$K^-\pi^+$	8.8%		
	$K^-\pi^+\pi^0$	4.8%	3.5%	9.8%
	$K^-\pi^+\pi^+\pi^-$	5.3%		

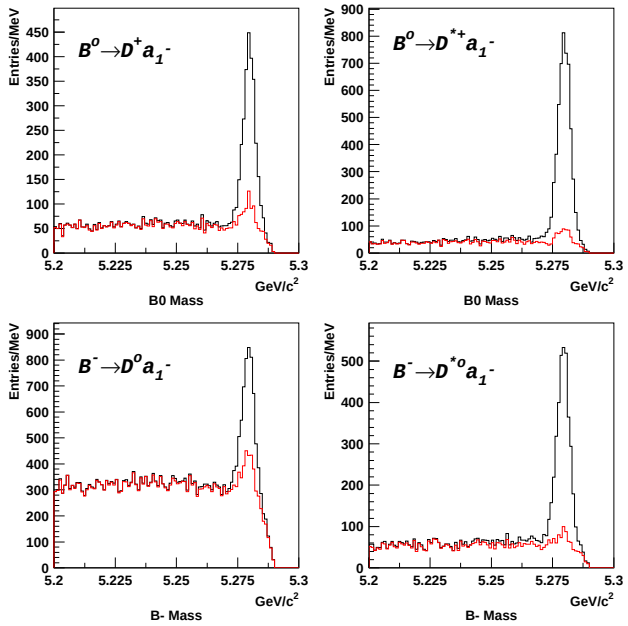

FIG. 8. Peaking background of non-resonant modes (dotted/colored line) underlays the signal of $B \to D^{(*)}a_1$ ($B\bar{B}$ Monte Carlo data, with $m_{\rho^0\pi} < 4.0$ GeV/c^2).

B. Non-resonant modes $B \to D^{(*)}\rho^0\pi$ and $B \to D^{(*)}\pi\pi\pi$

For the decays of $B \to D^{(*)}\rho^0\pi$ and $B \to D^{(*)}\pi\pi\pi$, the invariant masses of $\rho^0\pi$ and $\pi\pi\pi$ are required to be less than 4.0 GeV/c^2 and center of mass momenta of $\rho^0\pi$ and $\pi\pi\pi$ greater than 0.5 GeV/c. The m_{ES} distributions for $B \to D^{(*)}\rho^0\pi$ are shown in Fig. 9.

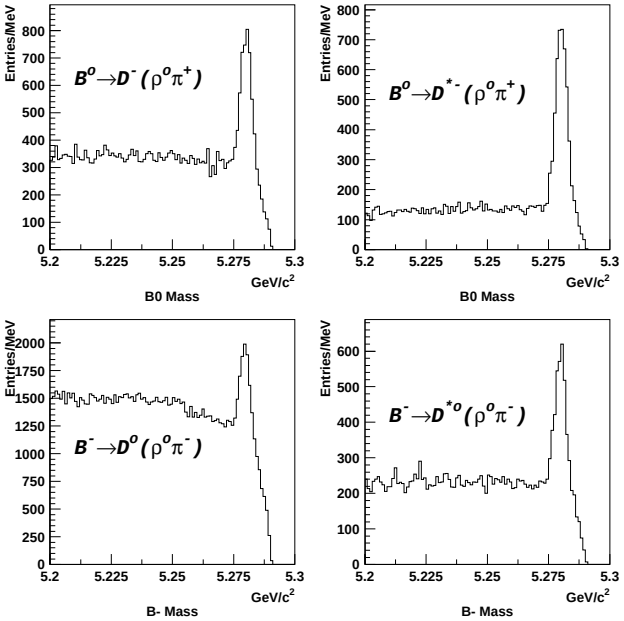

FIG. 9. Distribution of m_{ES} for $B \to D^{(*)}\rho^0\pi$.

The B signal region of $B \to D^{(*)}\rho^0\pi$, which is $|m_{ES} - 5.280\ \mathrm{GeV/c^2}| < 3\sigma_{m_{ES}}$ and $|\Delta E| < 2.5\sigma_{\Delta E}$ (see Fig. 9) also contains $B \to D^{(*)}a_1$ and $B \to D^{(*)}\pi\pi\pi$ candidates. Monte Carlo study shows that the $\pi\pi\pi$ invariant mass spectra for $B \to D^{(*)}\rho^0\pi^-$ and $B \to D^{(*)}\pi^-\pi^+\pi^-$ are different. But when the cuts $|m_{\pi^+\pi^-} - 0.77\ \mathrm{GeV/c^2}| < 0.15\ \mathrm{GeV/c^2}$ and center of mass momentum of $\pi^-\pi^+\pi^-$ greater than 0.5 GeV/c are applied to both modes, the $\pi^-\pi^+\pi^-$ mass spectra for $B \to D^{(*)}\rho^0\pi^-$ and $B \to D^{(*)}\pi^-\pi^+\pi^-$ are almost the same, as shown in Fig. 10. So, we can use the $\pi^-\pi^+\pi^-$ spectra of $B \to D^{(*)}\rho^0\pi$ to represent the spectra of $B \to D^{(*)}\pi^-\pi^+\pi^-$. Monte Carlo also shows that the $\pi^-\pi^+\pi^-$ spectra of modes $B^0 \to D^-\rho^0\pi^+$, $B^0 \to D^{*-}\rho^0\pi^+$, $B^- \to D^0\rho^0\pi^-$ and $B^- \to D^{*0}\rho^0\pi^-$ are quite similar because they have similar topology and kinematics (see Fig. 11).

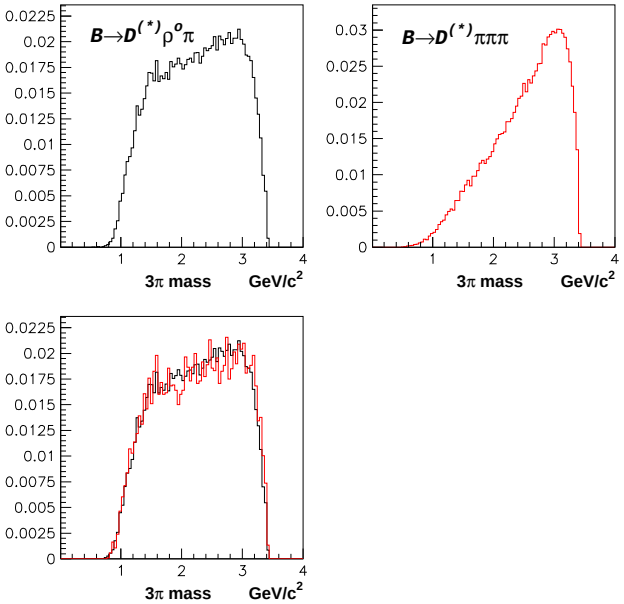

FIG. 10. Monte Carlo simulated distributions of $\pi^-\pi^+\pi^-$ mass for $B \to D^{(*)}\rho^0\pi^-$ (upper left), $B \to D^{(*)}\pi^-\pi^+\pi^-$ (upper right) and $\pi^-\pi^+\pi^-$ mass (lower left) for $B \to D^{(*)}\rho^0\pi^-$ (solid-line) and $B \to D^{(*)}\pi^-\pi^+\pi^-$ (dotted/colored-line) with the cuts $|m_{\pi^+\pi^-} - 0.77\ \mathrm{GeV/c^2}| < 0.15\ \mathrm{GeV/c^2}$ and center of mass momentum $p^*_{\pi^-\pi^+\pi^-} > 0.5$ GeV/c. (Normalized distributions with arbitrary unit in the vertical axis).

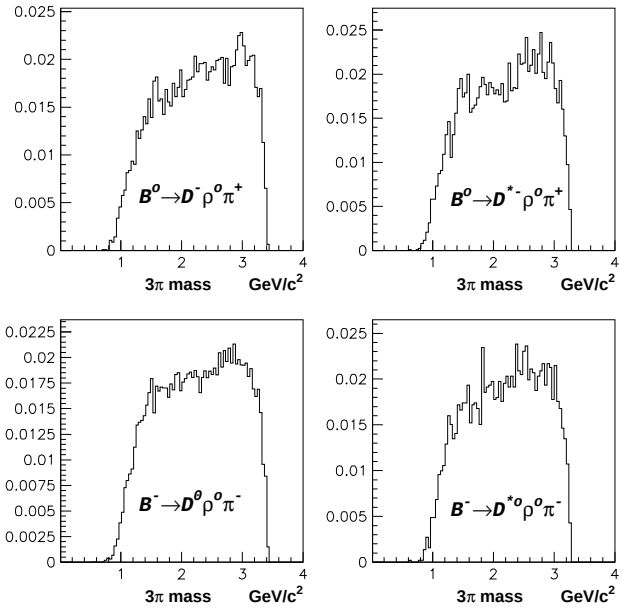

FIG. 11. Monte Carlo simulated $\rho^0\pi^+$ mass distribution for decay $B^0 \to D^-\rho^0\pi^+$, $B^0 \to D^{*-}\rho^0\pi^+$, $B^- \to D^0\rho^0\pi^-$, and $B^- \to D^{*0}\rho^0\pi^-$. (Normalized distributions with arbitrary unit in the vertical axis).

The invariant mass distributions of $\rho^0\pi^+$ in the B signal region are shown in Fig. 12. The shaded areas in the figures are the distributions from m_{ES} sideband region ($5.22\ \mathrm{GeV/c^2} < m_{ES} < 5.26\ \mathrm{GeV/c^2}$), and were scaled with the ratio of the integral of the Argus function in the m_{ES} sideband region to the integral in the m_{ES} signal region.

To estimate the fraction of $a_1(1260)$ in the $\rho^0\pi^-$ mass distribution, the $\rho^0\pi^-$ mass distribution, with the m_{ES} sideband background subtracted, are fitted to a Breit-Wigner distribution as $a_1(1260)$ signal plus the distribution of non-resonant $\rho^0\pi^+$ mass. The fits of B^0 modes are shown in Fig. 13. The non-resonant $\rho^0\pi^+$ mass distribution are from the reconstruction of the $\rho^0\pi^+$ mass in signal $B \to D^{(*)}\rho^0\pi^+$ Monte Carlo data. It is found that the $a_1(1260)$ signal is dominant in the mass spectra of $\rho^0\pi^+$ in both B^0 and B^- decay; therefore, the decay of $B \to D^{(*)}a_1(1260)$ is dominant in B decay with final state $D^{(*)}\rho^0\pi$. To separate the non-resonant mode $B \to D^{(*)}\rho^0\pi$ and $B \to D^{(*)}\pi\pi\pi$, a Dalitz plot analysis will be important.

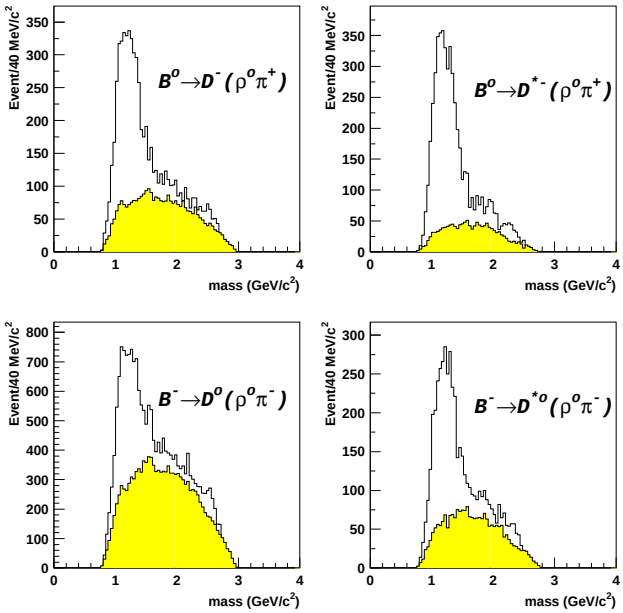

FIG. 12. $\rho^0\pi$ mass distribution in the m_{ES} signal region with the shaded area showing the m_{ES} sideband background.

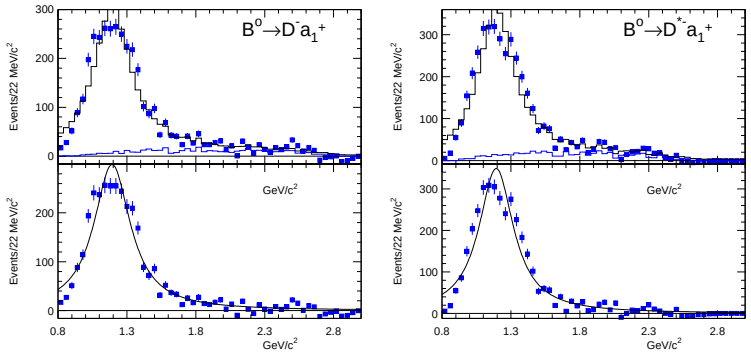

FIG. 13. Background-subtracted $\rho^0\pi$ mass spectra of data (dots) are fitted to a Breit-Wigner function as $a_1(1260)$ signal, plus the non-resonant $\rho^0\pi$ distribution as background. Lower plots show the non-resonant component subtracted a_1 mass.

IV. SUMMARY

The hadronic decay of $B \to D^{(*)}a_1(1260)$ and non-resonant modes $B \to D^{(*)}\rho^0\pi$, $B \to D^{(*)}\pi\pi\pi$ are studied with a large data sample. The preliminary result shows that $B \to D^{(*)}a_1(1260)$ is dominant in B decays with the final state $D^{(*)}\rho^0\pi$. The errors on the branching fraction measurements are estimated and improved compared with previous measurements. Further study is ongoing and final results will be published soon.

V. ACKNOWLEDGMENTS

We are grateful for the excellent luminosity and machine conditions provided by our PEP-II colleagues. The collaborating institutions wish to thank SLAC for its support and kind hospitality. This work is supported by DOE and NSF (USA), NSERC (Canada), IHEP (China), CEA and CNRS-IN2P3 (France), BMBF and DFG (Germany), INFN (Italy), FOM (The Netherlands), NFR (Norway), MIST (Russia), and PPARC (United Kingdom). Individuals have received support from the A. P. Sloan Foundation, Research Corporation, and Alexander von Humboldt Foundation.

[1] M. Bauer, B. Stech, and M. Wirbel, Z. Phys. C **29**, 637 (1985).
[2] M. Neubert and B. Stech, hep-ph/9705292.
[3] CLEO Collaboration, T. Coan *et al.*, Phys. Rev. Lett. **88**, 062001 (2002).
[4] Belle Collaboration, K. Abe *et al.*, Phys. Rev. Lett. **88**, 052002 (2002).
[5] P. F. Harrison and H. R. Quinn (ed.), The *BABAR* Physics Book, Chap. 6,7 (1998).
[6] M. Gronau, Pramana **62**, 255 (2004).
[7] CLEO Collaboration, D. Bortoletto *et al.*, Phys. Rev. Lett **69**, 2046 (1992).
[8] ARGUS Collaboration, Z. Phys. C **48** 543 (1990).
[9] CLEO Collaboration, M. S. Alam *et al.*, Phys. Rev. D **50**, 43 (1994).
[10] CLEO Collaboration, "Exclusive Reconstruction of $B \to D^{(*)}(n\pi)^-$ Decays," CLEO CONF 97-01, EPS 97-339.
[11] Review of Particle Physics, K. Hagiwara *et al.*, Phys. Rev. D **66**, 010001 (2002).
[12] P. Oddone, Annals N. Y. Acad. Sci. **578**, 237 (1989); PEP-II Conceptual Design Report, SLAC-R-418 (1993).
[13] *BABAR* Collaboration, B. Aubert *et al.*, Nucl. Instrum. Meth. A **479**, 1 (2002).
[14] UA1 Collaboration, C. Albajar *et al.*, Phys. Lett. B **186**, 247 (1987);
ARGUS Collaboration, H. Albrecht *et al.,* Phys. Lett, B **192**, 245 (1987).
[15] *BABAR* Collaboration, P. Burchat, Nucl. Instrum. Meth. A **342**, 292 (1994);
BABAR Collaboration, V. Re *et al.,* IEEE Trans. Nucl. Sci **49**, 3284 (2002).
[16] *BABAR* Collaboration, P. Burchat, J. Hiser, A. Boyarski, and D. Briggs, Nucl. Instrum. Meth. A **316**, 217 (1992);
BABAR Collaboration, G. Sciolla *et al.,* Nucl. Instrum. Meth. A **419**, 310 (1998).
[17] *BABAR* Collaboration, J. Schwiening *et al.,* Nucl. Instrum. Meth. A **502**, 67 (2003).
[18] *BABAR* Collaboration, R. J. Barlow *et al.,* Nucl. Instrum. Meth. A **420**, 162 (1999).
[19] G. C. Fox and S. Wolfram, Phys. Rev. Lett. **41**, 1581 (1978).
[20] ARGUS Collaboration, H. Albrecht *et al.*, Phys. Lett. B **185**, 218 (1987).
[21] E691 Collaboration, J. C. Anjos *et al.*, Phys. Rev. Lett. **62**, 1717 (1989).